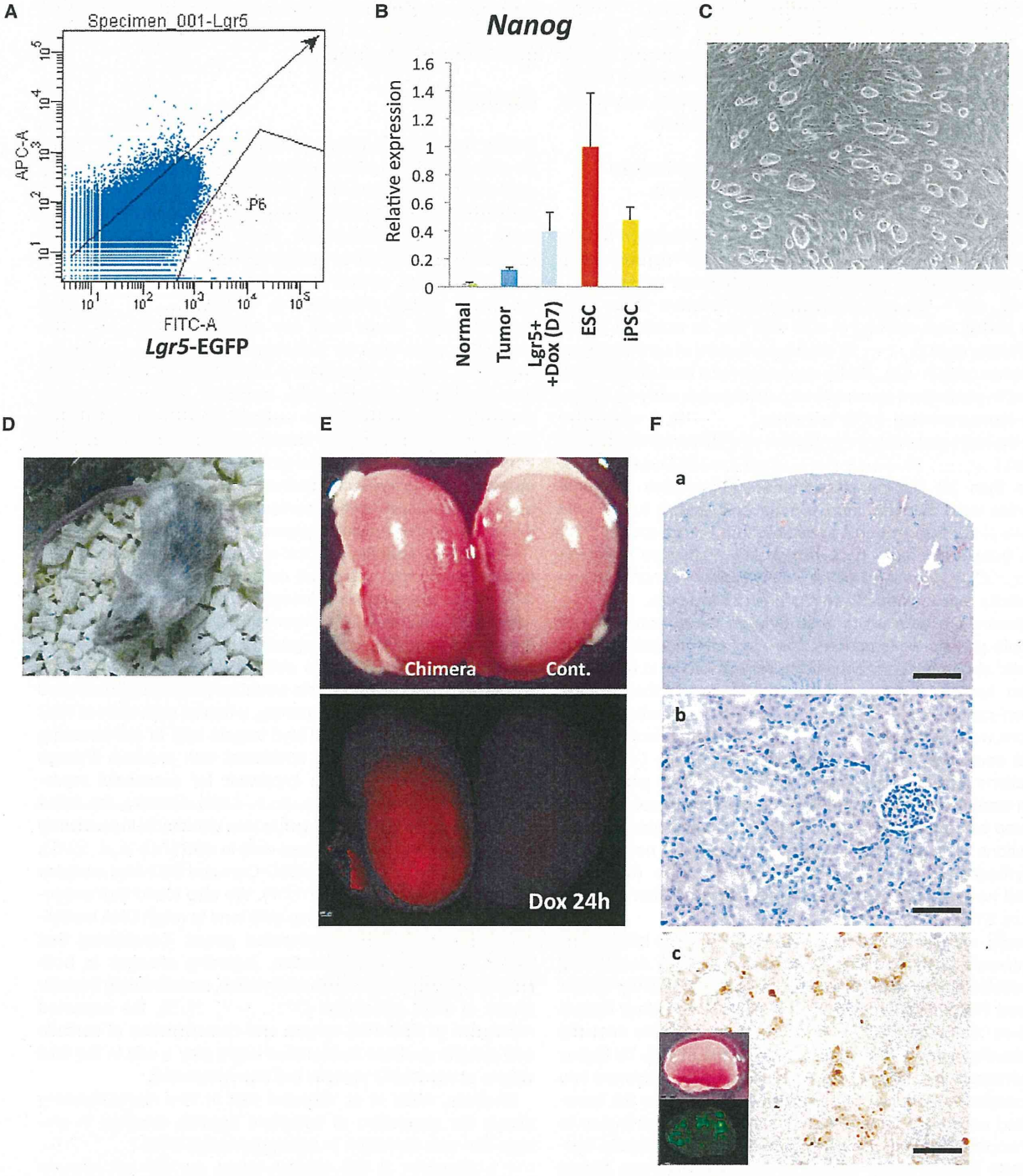

Figure 6. Generation of iPSCs from Dox-Withdrawn Tumors and Their Contribution to Normal-Looking Kidney Tissue

(A) The fluorescence-activated cell sorting analyses of Dox-withdrawn kidney tumor cells in a reprogrammable chimeric mouse with the *Lgr5*-EGFP reporter. GFP-positive *Lgr5*-expressing cells were sorted to exclusively isolate Dox-withdrawn tumor cells.

(B) Dox treatment of *Lgr5*-expressing tumor cells caused the rapid induction of *Nanog*. The *Nanog* levels were examined after seven days of treatment with Dox in vitro. Data are presented as mean ± SD. The level in ESCs was set to 1.

(C) An image of iPSCs derived from *Lgr5*-positive kidney tumor cells.

(legend continued on next page)

Furthermore, teratoma-derived in vivo iPSCs in this study failed to differentiate into placental tissues despite robust fetal contribution upon injection into eight-cell-stage embryos (data not shown), suggesting that not all in vivo iPSCs are totipotent. Because the previous study was conducted using circulating iPSCs recovered in blood, the cell of origin for in vivo reprogramming might affect the acquisition of totipotent features. It should be also noted that Abad et al. utilized germline-transmitted transgenic mice that harbor lentivirus-mediated integration of inducible reprogramming factors (Carey et al., 2009) whereas we examined chimeric mice with transgenes at a targeted locus. The different levels of transgene induction caused by such distinct transgenic systems may underlie differences in the phenotypes observed between these two studies.

Here, we show that failed reprogramming-associated cancers resemble Wilms tumors in terms of histology and molecular characteristics, including aberrant expression of imprinted genes correlated with altered DNA methylation. It is well known that Wilms tumors have characteristics distinct from adult kidney cancers in many aspects. On the basis of our findings in Dox-withdrawn tumors, we discovered that Wilms tumors harbor an activated ESC core regulatory circuitry. This is in sharp contrast to previous findings that most adult cancers do not show activation of ESC core regulatory circuitry (Kim et al., 2010). We also found that many ESC-PRC targets are not repressed in Wilms tumors, despite common repression in many cancers (Ben-Porath et al., 2008; Kim et al., 2010). Gene Ontology analysis revealed that derepressed PRC genes in Wilms tumors include genes involved in kidney development, whereas they are not enriched in derepressed PRC genes in RCCs (data not shown), suggesting that activation of the embryonic kidney transcriptional network is associated with Wilms tumor development. Taken together, strongly active ESC-core regulatory circuitry and derepression of certain ESC-PRC targets may characterize Wilms tumors and may account for the characteristics distinctive of Wilms tumors and adult kidney cancers.

Although we revealed striking similarity between Dox-withdrawn kidney tumors and Wilms tumors, it remains unclear whether reprogramming processes play a role in the development of human Wilms tumors. It has been widely accepted that nephrogenic rests, abnormally persistent clusters of embryonal cells, are the precursors of Wilms tumors. Considering the artificial expression of reprogramming factors in our experimental system, the current study does not provide direct evidence that dedifferentiation is normally involved in the human Wilms tumor development. Yet, based on our findings, it is conceivable that a reprogramming process might cause cell-fate conversion into progenitor-like states, leading to the development of nephrogenic rests required for the early stages of Wilms tumorigenesis. Further detailed analyses using human samples are required to uncover the role of reprogramming in cancer development in humans.

In summary, we demonstrated that premature termination of in vivo reprogramming causes tumor development resembling Wilms tumor. Our findings suggest that altered epigenetic regulations relating to somatic cell reprogramming drive tumorigenesis, highlighting the importance of epigenetic regulation in cancer development.

EXPERIMENTAL PROCEDURES

Generation of OSMK-Inducible ESCs

A 7 kb fragment containing Oct3/4-P2A-Sox2-T2A-Klf4-E2A-c-Myc-ires-mCherry cDNA was generated (Carey et al., 2009) and ligated into the pBS31 vector (Beard et al., 2006). The resulting construct was electroporated into KH2 ESCs to obtain OSKM-inducible ESCs (Beard et al., 2006). OKS-, KMS-, O-, LacZ-inducible ESCs were also generated using the KH2 ESCs system.

Mice

Chimeric mice were generated using reprogramming factor-inducible ESCs by diploid blastocyst injection. *Lgr5-EGFP-ires-CreERT2* mice were obtained from The Jackson Laboratory and were crossed with OSKM-inducible mice to obtain embryos. The compound transgenic MEFs were treated with Dox to establish the OSKM-inducible iPSCs with the *Lgr5-EGFP* reporter allele. All animal experiments were approved by the CiRA Animal Experiment Committee, and the care of the animals was in accordance with institutional guidelines.

Doxycycline Treatment

Mice at 4 or 14 weeks of age were administered 2 mg/ml Dox in their drinking water supplemented with 10 mg/ml sucrose. For cell culture, Dox was used at a concentration of 2 μg/ml.

Secondary Tumor Development

Primary kidney tumors were minced and treated with collagenase (1 U/ml) followed by 0.25% trypsin digestion. The dissociated tumor cells were inoculated subcutaneously into BALB/cSlc-*nu/nu* mice or C.B-17/Icr-*scid*Jcl mice to form transplanted secondary tumors.

RNA Preparation, qRT-PCR and Microarray Analysis

Total RNA was isolated using the RNeasy Plus Mini kit (QIAGEN). The quantitative real-time PCR analysis was performed using the GoTaq qPCR Master Mix (Promega). The specific primer pairs used for amplification are shown in Table S2. The transcript levels were normalized to the *β-actin* level. The microarray analysis was performed using the Mouse Gene 1.0 ST Array (Affymetrix) in accordance with the manufacturer's instructions. All of the data analyses were performed using the GeneSpring GX software program (version 12; Agilent Technology).

DNA Methylation Analyses

The RRBS analysis was performed as described previously (Boyle et al., 2012). The samples were sequenced on an Illumina HiSeq 2000 machine. Three-kilobase regions flanking transcription start site (from −1,500 to +1,500) were analyzed to examine DNA methylation levels. The DNA methylation levels for each gene were determined based on the median of DNA methylation values at CpG sites within the region. The DNA methylation values at CpG sites

(D) Kidney tumor-derived iPSCs can contribute to adult chimeric mice.
(E) No tumor formation was observed in the kidneys of chimeric mice generated with kidney tumor-derived iPSCs. Note that Dox treatment for 24 hr confirmed the contribution of kidney-tumor-derived iPSCs to the normal-looking kidney.
(F) The histological analyses of the kidneys of chimeric mice demonstrated no detectable histological abnormalities (a and b). Kidney-tumor-derived iPSCs labeled with Venus could contribute to normal-looking kidney (c). Scale bars, 500 μm (a) and 100 μm (b, c).
See also Figure S7.

containing higher than 10× coverage in all comparative samples were used for the analysis.

Histological Analysis and Immunostaining

Normal and tumor tissue samples were fixed in 10% buffered formalin for 24 hr and embedded in paraffin. Sections (4 μm) were stained with hematoxylin and eosin (H&E), and serial sections were used for the immunohistochemical analyses. The primary antibodies used were anti-Oct3/4 (1:100 dilution; BD Biosciences), anti-Ki-67 (1:100 dilution; Dako), anti-insulin (1:500 dilution; Dako), anti-BrdU (1:500 dilution; Abcam), anti-2A (1:250 dilution; Millipore), anti-Lin28b (1:100 dilution; Cell Signaling Technology), and anti-GFP (1:500 dilution; Invitrogen).

ACCESSION NUMBERS

The Gene Expression Omnibus accession number for the microarray and RRBS data reported in this paper is GSE52304.

SUPPLEMENTAL INFORMATION

Supplemental Information includes Extended Experimental Procedures, seven figures, and three tables and can be found with this article online at http://dx.doi.org/10.1016/j.cell.2014.01.005.

ACKNOWLEDGMENTS

We are grateful to T. Taya for CGH analysis and S. Sakurai and T. Sato for RRBS analysis. We also thank S. Masui, H. Sakurai, and members in Yamada laboratory for helpful discussions and T. Ukai, K. Osugi, and N. Nishimoto for assistance. The authors were supported in part by a Grant-in-Aid from the Ministry of Education, Culture, Sports, Science, and Technology of Japan (MEXT); the Ministry of Health, Labor, and Welfare of Japan; the JST; the Funding Program for World-Leading Innovative R&D on Science and Technology (FIRST Program) of the Japanese Society for the Promotion of Science (JSPS); the Takeda Science Foundation; and the Naito Foundation. S.Y. is a member without salary of the scientific advisory boards of iPierian, iPS Academia Japan, Megakaryon Corporation, and HEALIOS K. K. Japan. The iCeMS is supported by World Premier International Research Center Initiative, MEXT, Japan.

Received: May 29, 2013
Revised: November 6, 2013
Accepted: January 3, 2014
Published: February 13, 2014

REFERENCES

Abad, M., Mosteiro, L., Pantoja, C., Cañamero, M., Rayon, T., Ors, I., Graña, O., Megías, D., Domínguez, O., Martínez, D., et al. (2013). Reprogramming in vivo produces teratomas and iPS cells with totipotency features. Nature *502*, 340–345.

Aiden, A.P., Rivera, M.N., Rheinbay, E., Ku, M., Coffman, E.J., Truong, T.T., Vargas, S.O., Lander, E.S., Haber, D.A., and Bernstein, B.E. (2010). Wilms tumor chromatin profiles highlight stem cell properties and a renal developmental network. Cell Stem Cell *6*, 591–602.

Barker, N., van Es, J.H., Kuipers, J., Kujala, P., van den Born, M., Cozijnsen, M., Haegebarth, A., Korving, J., Begthel, H., Peters, P.J., and Clevers, H. (2007). Identification of stem cells in small intestine and colon by marker gene Lgr5. Nature *449*, 1003–1007.

Barker, N., Rookmaaker, M.B., Kujala, P., Ng, A., Leushacke, M., Snippert, H., van de Wetering, M., Tan, S., Van Es, J.H., Huch, M., et al. (2012). Lgr5(+ve) stem/progenitor cells contribute to nephron formation during kidney development. Cell Rep. *2*, 540–552.

Beard, C., Hochedlinger, K., Plath, K., Wutz, A., and Jaenisch, R. (2006). Efficient method to generate single-copy transgenic mice by site-specific integration in embryonic stem cells. Genesis *44*, 23–28.

Ben-Porath, I., Thomson, M.W., Carey, V.J., Ge, R., Bell, G.W., Regev, A., and Weinberg, R.A. (2008). An embryonic stem cell-like gene expression signature in poorly differentiated aggressive human tumors. Nat. Genet. *40*, 499–507.

Boyle, P., Clement, K., Gu, H., Smith, Z.D., Ziller, M., Fostel, J.L., Holmes, L., Meldrim, J., Kelley, F., Gnirke, A., and Meissner, A. (2012). Gel-free multiplexed reduced representation bisulfite sequencing for large-scale DNA methylation profiling. Genome Biol. *13*, R92.

Brambrink, T., Foreman, R., Welstead, G.G., Lengner, C.J., Wernig, M., Suh, H., and Jaenisch, R. (2008). Sequential expression of pluripotency markers during direct reprogramming of mouse somatic cells. Cell Stem Cell *2*, 151–159.

Carey, B.W., Markoulaki, S., Hanna, J., Saha, K., Gao, Q., Mitalipova, M., and Jaenisch, R. (2009). Reprogramming of murine and human somatic cells using a single polycistronic vector. Proc. Natl. Acad. Sci. USA *106*, 157–162.

Carey, B.W., Markoulaki, S., Beard, C., Hanna, J., and Jaenisch, R. (2010). Single-gene transgenic mouse strains for reprogramming adult somatic cells. Nat. Methods *7*, 56–59.

Ehrich, M., Nelson, M.R., Stanssens, P., Zabeau, M., Liloglou, T., Xinarianos, G., Cantor, C.R., Field, J.K., and van den Boom, D. (2005). Quantitative high-throughput analysis of DNA methylation patterns by base-specific cleavage and mass spectrometry. Proc. Natl. Acad. Sci. USA *102*, 15785–15790.

Folmes, C.D., Nelson, T.J., Martinez-Fernandez, A., Arrell, D.K., Lindor, J.Z., Dzeja, P.P., Ikeda, Y., Perez-Terzic, C., and Terzic, A. (2011). Somatic oxidative bioenergetics transitions into pluripotency-dependent glycolysis to facilitate nuclear reprogramming. Cell Metab. *14*, 264–271.

Fussner, E., Djuric, U., Strauss, M., Hotta, A., Perez-Iratxeta, C., Lanner, F., Dilworth, F.J., Ellis, J., and Bazett-Jones, D.P. (2011). Constitutive heterochromatin reorganization during somatic cell reprogramming. EMBO J. *30*, 1778–1789.

Hochedlinger, K., Yamada, Y., Beard, C., and Jaenisch, R. (2005). Ectopic expression of Oct-4 blocks progenitor-cell differentiation and causes dysplasia in epithelial tissues. Cell *121*, 465–477.

Hong, H., Takahashi, K., Ichisaka, T., Aoi, T., Kanagawa, O., Nakagawa, M., Okita, K., and Yamanaka, S. (2009). Suppression of induced pluripotent stem cell generation by the p53-p21 pathway. Nature *460*, 1132–1135.

Jones, P.A., and Baylin, S.B. (2002). The fundamental role of epigenetic events in cancer. Nat. Rev. Genet. *3*, 415–428.

Kim, J., Woo, A.J., Chu, J., Snow, J.W., Fujiwara, Y., Kim, C.G., Cantor, A.B., and Orkin, S.H. (2010). A Myc network accounts for similarities between embryonic stem and cancer cell transcription programs. Cell *143*, 313–324.

Kobayashi, A., Valerius, M.T., Mugford, J.W., Carroll, T.J., Self, M., Oliver, G., and McMahon, A.P. (2008). Six2 defines and regulates a multipotent self-renewing nephron progenitor population throughout mammalian kidney development. Cell Stem Cell *3*, 169–181.

Maherali, N., Sridharan, R., Xie, W., Utikal, J., Eminli, S., Arnold, K., Stadtfeld, M., Yachechko, R., Tchieu, J., Jaenisch, R., et al. (2007). Directly reprogrammed fibroblasts show global epigenetic remodeling and widespread tissue contribution. Cell Stem Cell *1*, 55–70.

Meissner, A., Gnirke, A., Bell, G.W., Ramsahoye, B., Lander, E.S., and Jaenisch, R. (2005). Reduced representation bisulfite sequencing for comparative high-resolution DNA methylation analysis. Nucleic Acids Res. *33*, 5868–5877.

Mikkelsen, T.S., Ku, M., Jaffe, D.B., Issac, B., Lieberman, E., Giannoukos, G., Alvarez, P., Brockman, W., Kim, T.K., Koche, R.P., et al. (2007). Genome-wide maps of chromatin state in pluripotent and lineage-committed cells. Nature *448*, 553–560.

Mikkelsen, T.S., Hanna, J., Zhang, X., Ku, M., Wernig, M., Schorderet, P., Bernstein, B.E., Jaenisch, R., Lander, E.S., and Meissner, A. (2008). Dissecting direct reprogramming through integrative genomic analysis. Nature *454*, 49–55.

Ogawa, O., Eccles, M.R., Szeto, J., McNoe, L.A., Yun, K., Maw, M.A., Smith, P.J., and Reeve, A.E. (1993). Relaxation of insulin-like growth factor II gene imprinting implicated in Wilms' tumour. Nature *362*, 749–751.

Ohta, S., Nishida, E., Yamanaka, S., and Yamamoto, T. (2013). Global splicing pattern reversion during somatic cell reprogramming. Cell Rep. *5*, 357–366.

Okita, K., Ichisaka, T., and Yamanaka, S. (2007). Generation of germline-competent induced pluripotent stem cells. Nature *448*, 313–317.

Onder, T.T., Kara, N., Cherry, A., Sinha, A.U., Zhu, N., Bernt, K.M., Cahan, P., Marcarci, B.O., Unternaehrer, J., Gupta, P.B., et al. (2012). Chromatin-modifying enzymes as modulators of reprogramming. Nature *483*, 598–602.

Polo, J.M., Anderssen, E., Walsh, R.M., Schwarz, B.A., Nefzger, C.M., Lim, S.M., Borkent, M., Apostolou, E., Alaei, S., Cloutier, J., et al. (2012). A molecular roadmap of reprogramming somatic cells into iPS cells. Cell *151*, 1617–1632.

Rais, Y., Zviran, A., Geula, S., Gafni, O., Chomsky, E., Viukov, S., Mansour, A.A., Caspi, I., Krupalnik, V., Zerbib, M., et al. (2013). Deterministic direct reprogramming of somatic cells to pluripotency. Nature *502*, 65–70.

Samavarchi-Tehrani, P., Golipour, A., David, L., Sung, H.K., Beyer, T.A., Datti, A., Woltjen, K., Nagy, A., and Wrana, J.L. (2010). Functional genomics reveals a BMP-driven mesenchymal-to-epithelial transition in the initiation of somatic cell reprogramming. Cell Stem Cell *7*, 64–77.

Sridharan, R., Tchieu, J., Mason, M.J., Yachechko, R., Kuoy, E., Horvath, S., Zhou, Q., and Plath, K. (2009). Role of the murine reprogramming factors in the induction of pluripotency. Cell *136*, 364–377.

Stadtfeld, M., Apostolou, E., Akutsu, H., Fukuda, A., Follett, P., Natesan, S., Kono, T., Shioda, T., and Hochedlinger, K. (2010a). Aberrant silencing of imprinted genes on chromosome 12qF1 in mouse induced pluripotent stem cells. Nature *465*, 175–181.

Stadtfeld, M., Maherali, N., Borkent, M., and Hochedlinger, K. (2010b). A reprogrammable mouse strain from gene-targeted embryonic stem cells. Nat. Methods *7*, 53–55.

Steenman, M.J., Rainier, S., Dobry, C.J., Grundy, P., Horon, I.L., and Feinberg, A.P. (1994). Loss of imprinting of IGF2 is linked to reduced expression and abnormal methylation of H19 in Wilms' tumour. Nat. Genet. *7*, 433–439.

Takahashi, K., and Yamanaka, S. (2006). Induction of pluripotent stem cells from mouse embryonic and adult fibroblast cultures by defined factors. Cell *126*, 663–676.

Takahashi, K., Tanabe, K., Ohnuki, M., Narita, M., Ichisaka, T., Tomoda, K., and Yamanaka, S. (2007). Induction of pluripotent stem cells from adult human fibroblasts by defined factors. Cell *131*, 861–872.

Tchieu, J., Kuoy, E., Chin, M.H., Trinh, H., Patterson, M., Sherman, S.P., Aimiuwu, O., Lindgren, A., Hakimian, S., Zack, J.A., et al. (2010). Female human iPSCs retain an inactive X chromosome. Cell Stem Cell *7*, 329–342.

Wernig, M., Meissner, A., Foreman, R., Brambrink, T., Ku, M., Hochedlinger, K., Bernstein, B.E., and Jaenisch, R. (2007). In vitro reprogramming of fibroblasts into a pluripotent ES-cell-like state. Nature *448*, 318–324.

Woltjen, K., Michael, I.P., Mohseni, P., Desai, R., Mileikovsky, M., Hämäläinen, R., Cowling, R., Wang, W., Liu, P., Gertsenstein, M., et al. (2009). piggyBac transposition reprograms fibroblasts to induced pluripotent stem cells. Nature *458*, 766–770.

Yamada, Y., Jackson-Grusby, L., Linhart, H., Meissner, A., Eden, A., Lin, H., and Jaenisch, R. (2005). Opposing effects of DNA hypomethylation on intestinal and liver carcinogenesis. Proc. Natl. Acad. Sci. USA *102*, 13580–13585.

Yusenko, M.V., Kuiper, R.P., Boethe, T., Ljungberg, B., van Kessel, A.G., and Kovacs, G. (2009). High-resolution DNA copy number and gene expression analyses distinguish chromophobe renal cell carcinomas and renal oncocytomas. BMC Cancer *9*, 152.

Development 140, 66-75 (2013) doi:10.1242/dev.084103

Dose-dependent roles for canonical Wnt signalling in *de novo* crypt formation and cell cycle properties of the colonic epithelium

Akihiro Hirata[1,*], Jochen Utikal[2,3,*], Satoshi Yamashita[4], Hitomi Aoki[5], Akira Watanabe[6], Takuya Yamamoto[6], Hideyuki Okano[7], Nabeel Bardeesy[2], Takahiro Kunisada[5], Toshikazu Ushijima[4], Akira Hara[8], Rudolf Jaenisch[9], Konrad Hochedlinger[2,‡] and Yasuhiro Yamada[6,10,‡]

SUMMARY

There is a gradient of β-catenin expression along the colonic crypt axis with the highest levels at the crypt bottom. In addition, colorectal cancers show a heterogeneous subcellular pattern of β-catenin accumulation. However, it remains unclear whether different levels of Wnt signalling exert distinct roles in the colonic epithelium. Here, we investigated the dose-dependent effect of canonical Wnt activation on colonic epithelial differentiation by controlling the expression levels of stabilised β-catenin using a doxycycline-inducible transgenic system in mice. We show that elevated levels of Wnt signalling induce the amplification of Lgr5+ cells, which is accompanied by crypt fission and a reduction in cell proliferation among progenitor cells. By contrast, lower levels of β-catenin induction enhance cell proliferation rates of epithelial progenitors without affecting crypt fission rates. Notably, slow-cycling cells produced by β-catenin activation exhibit activation of Notch signalling. Consistent with the interpretation that the combination of Notch and Wnt signalling maintains crypt cells in a low proliferative state, the treatment of β-catenin-expressing mice with a Notch inhibitor turned such slow-cycling cells into actively proliferating cells. Our results indicate that the activation of the canonical Wnt signalling pathway is sufficient for *de novo* crypt formation, and suggest that different levels of canonical Wnt activations, in cooperation with Notch signalling, establish a hierarchy of slower-cycling stem cells and faster-cycling progenitor cells characteristic for the colonic epithelium.

KEY WORDS: Wnt signalling, Notch signalling, Intestinal stem cell, Mouse

INTRODUCTION

The intestinal epithelium is characterised by rapid and continuous renewal throughout life. One of the major players involved in the renewal of the intestinal epithelium is the canonical Wnt signalling pathway. Experimental manipulation of Wnt signalling has been shown to influence epithelial proliferation in the intestines (Korinek et al., 1998; Pinto et al., 2003; Kuhnert et al., 2004; Sansom et al., 2004; Andreu et al., 2005; Fevr et al., 2007). For example, inactivation of Wnt signalling by transgenic or adenoviral expression of *Dickkopf1* (*Dkk1*), a secreted Wnt inhibitor, leads to marked inhibition of epithelial proliferation in the intestines (Pinto et al., 2003; Kuhnert et al., 2004). By contrast, two independent groups have demonstrated that loss of *Apc* results in a rapid and dramatic enlargement of the crypt compartment associated with abnormal cell proliferation in the small intestine (Sansom et al., 2004; Andreu et al., 2005). Together, these experiments provide definitive evidence for the importance of Wnt signalling in controlling intestinal epithelial proliferation.

In addition to controlling cell proliferation, a role for Wnt/β-catenin signalling in stem cell maintenance in the intestine has been suggested. Inactivation of Wnt signalling by either overexpression of *Dkk1* or conditional deletion of *Ctnnb1* (the gene encoding β-catenin) results in the loss of intestinal crypts, indicating that Wnt signalling is indispensable for stem cell maintenance (Pinto et al., 2003; Kuhnert et al., 2004; Fevr et al., 2007). In fact, the intestinal stem cell (ISC) marker *Lgr5* has initially been identified as a target of β-catenin/Tcf transcription (Barker et al., 2007), which is in accordance with the view that ISCs harbour a higher activity of canonical Wnt signals. In further support of this notion, nuclear accumulation of β-catenin has been observed at the crypt bottom in cells that potentially include ISCs (van de Wetering et al., 2002).

The number of ISCs has to be tightly regulated in the intestinal crypts in order to facilitate tissue turnover but prevent abnormal growth. ISCs are usually involved in a process of homeostatic self-renewal in the adult intestine but can also be rapidly recruited to repair tissues after injury. Indirect evidence for an involvement of Wnt signalling in stem cell amplification derives from a study showing that PTEN deficiency increases the frequency of crypt fission/budding and the number of cells expressing *Musashi1*, a putative ISC marker, through activated Wnt signalling (He et al., 2007). However, the underlying mechanism by which activated Wnt signalling may expand ISCs remains elusive, and direct evidence

[1]Division of Animal Experiment, Life Science Research Center, Gifu University, 1-1 Yanagido, Gifu, 501-1194, Japan. [2]Massachusetts General Hospital Cancer Center and Center for Regenerative Medicine, Harvard Stem Cell Institute, 185 Cambridge Street, Boston, MA 02114, USA. [3]Skin Cancer Unit, German Cancer Research Center, Heidelberg, Germany and Department of Dermatology, Venereology and Allergology, University Medical Center Mannheim, Ruprecht-Karl University of Heidelberg, Mannheim, Germany. [4]Division of Epigenomics, National Cancer Center Research Institute, 5-1-1 Tsukiji, Chuo-ku, Tokyo, Japan. [5]Department of Tissue and Organ Development and [8] Department of Tumor Pathology, Gifu University Graduate School of Medicine, 1-1 Yanagido, Gifu, 501-1194, Japan. [6]Center for iPS Cell Research and Application (CiRA), Institute for Integrated Cell-Material Sciences (WPI-iCeMS), Kyoto University, 53 Kawahara-cho, Shogoin, Sakyo-ku, Kyoto 606-8507, Japan. [7]Department of Physiology, Keio University School of Medicine, 35 Shinanomach, Shinjuku-ku, Tokyo 160-8582, Japan. [9]Whitehead Institute for Biomedical Research, Massachusetts Institute of Technology, Cambridge, MA 02142, USA. [10]PRESTO, Japan Science and Technology Agency, Saitama, Japan.

*These authors contributed equally to this work
‡Authors for correspondence (khochedlinger@helix.mgh.harvard.edu; y-yamada@cira.kyoto-u.ac.jp)

Accepted 15 October 2012

that elevated Wnt signalling is sufficient for stem cell expansion in the adult intestine is lacking.

Disruption of canonical Wnt signalling is involved in the vast majority of colon cancers. Mutation in *APC* or *CTNNB1* is the initiating event in the transformation of colonic epithelial cells, which lead to the constitutive activation of Wnt signalling. Importantly, despite the presence of the activating mutations for Wnt signalling, colorectal cancers show cellular heterogeneity of β-catenin accumulation within a tumour mass. Immunohistochemical studies have revealed that nuclear β-catenin accumulation, the hallmark of activated Wnt signalling, is observed in a subset of colon tumour cells (Brabletz et al., 2001; Jung et al., 2001; Fodde and Brabletz, 2007). Furthermore, a recent study indicates that colon tumour cells with high Wnt signalling activity show the properties of cancer stem cells (Vermeulen et al., 2010), which emphasises the need for further studies on the dose-dependent effect of Wnt signalling on intestinal epithelial cells.

Although a large body of literature has established that activation of the canonical Wnt signalling is the dominant force in the maintenance of intestinal homeostasis, other signalling cascades, such as the Notch, BMP and PI3 cascades, have also been implicated in the control of epithelial cell proliferation and stem cell turnover (Scoville et al., 2008). However, it remains poorly understood how these other signalling cascades integrate with Wnt signalling in the intestinal epithelium to control stem cell turnover and epithelial regeneration. It is assumed that the various signalling cascades act in a hierarchical manner, and regulate each other. A better understanding of how the coordinated activity of these signalling cascades maintains intestinal homeostasis is crucial for dissecting the mechanisms of ISCs as well as for attempts to utilise stem cells in regenerative medicine and to target them in diseases such as cancer.

Using a novel β-catenin-inducible mouse model, we show here that elevated levels of activated β-catenin induces *de novo* crypt formation but reduces epithelial cell proliferation among progenitors. However, combined β-catenin overexpression and Notch inhibition turns these slow-cycling cells into proliferating cells. These results imply that β-catenin signalling fulfils dual roles in the control of intestinal epithelial regeneration by (1) promoting crypt formation and (2) activating cell proliferation in cooperation with Notch signalling.

MATERIALS AND METHODS

Mice

Transgenic mice expressing histone H2B-green fluorescent protein (H2B-GFP) fusion protein under the control of a TRE were obtained from Jackson Laboratories [Bar Harbor, ME, USA; strain name: Tg(tetO-HIST1H2BJ/GFP)47Efu] and crossed with mice harbouring a ROSA26 promoter-driven M2rtTA allele (Beard et al., 2006). β-Catenin embryonic stem (ES) cell line was generated with stabilised β-catenin (S33 mutation) cDNA (Morin et al., 1977; van Noort et al., 2002) with use of KH2 ES cell line and injected into blastocysts to produce transgenic mice. Mice of 4 to 8 weeks of age were fed 0.1 or 2.0 mg/ml doxycycline in the drinking water supplemented with 10 mg/ml sucrose. *Lgr5-GFP* knock-in mouse were obtained from Jackson Laboratories (strain name: B6.129P2-*Lgr5*$^{tm1(cre/ESR1)Cle}$/J).

Crypt isolation

Crypts were isolated form the whole colon and caecum by incubation in Hanks' balanced salt solution containing 30 mM EDTA as described previously (Tsukamoto et al., 2001).

Flow cytometry

Isolated crypts were incubated in 1% collagenase type 1 for 15 minutes at 37°C and then 0.25% trypsin/1m M EDTA for 5 minutes at 37°C. Single-cell suspensions were obtained by transfer through nylon mesh to remove large clumps, washing, and resuspension in staining medium containing 0.5 μl/ml propidium iodide (Calbiochem-Novabiochem Corp., San Diego, CA, USA) to eliminate dead cells. The cells were sorted by fluorescence-activated cell sorting (FACS) using a Vantage SE flow cytometer (Becton Dickinson, San Jose, CA, USA).

Microarray analysis

Total RNA was extracted from isolated crypts or FACS-sorted cells as previously reported (Yamashita et al., 2003). Oligonucleotide microarray hybridisation and scanning using GeneChip Mouse Genome 430 2.0 Array (Affimetrix) were performed as previously reported (Yamashita et al., 2003). For the pathway analysis, 907 probe sets, which are specifically upregulated in β-catenin induced cells, but not in H2B-low fast-cycling cells, were selected. The gene enrichment analysis was performed with DAVID PANTHER annotation tool. Microarray data have been deposited in Gene Expression Omnibus database under accession number GSE41688.

Quantitative real-time RT-PCR

qRT-PCR was performed as described previously (Oyama et al., 2008). The expression level of each gene was normalised to the β-actin expression level using the standard curve method. Each experiment was done in either duplicate or triplicate, and then, the average was calculated. Primer sequences for qPCR were taken from PrimerBank. The primer sequences are listed in supplementary material Table S2.

Histological and immunohistochemical analysis

Normal and tumour tissue samples were fixed in 10% buffered formalin, proceeded by standard method and embedded in paraffin. Sections were stained with Haematoxylin and Eosin (H&E), and serial sections were used for immunohistochemical analysis. Immunostaining was performed as described previously (Oyama et al., 2008) using the following antibodies: anti-β-catenin (1:1000 dilution; BD Transduction Laboratories, San Diego, CA, USA), anti-Musashi-1 [1:500 dilution (Kaneko et al., 2000)], anti-BrdU (1:250 dilution; Abcam, Cambridge, UK), anti-Hes1 [1:100 dilution; a gift from Dr Sudo (Ito et al., 2000)], anti-GFP (1:1500 dilution; Invitrogen, Carlsbad, CA, USA), anti-Ki67 (1:250 dilution; Dako Corp., Carpinteria, CA, USA) and anti-chromogranin A (1:1500 dilution; Abcam). Photomicrographs show the distal part of the colon or caecum in the figures.

Bromodeoxyuridine (BrdU) assay

Mice were injected with BrdU intraperitoneally (i.p.) at a dose of 100 mg/kg body weight. Mice were sacrificed 2 or 48 hours after injection, and incorporated BrdU was detected by immunostaining with anti-BrdU antibody as described above.

Notch inhibitor

γ-Secretase inhibitor (MRK003-ONC) was kindly provided by Merck and administrated orally at 100 mg/kg 2 days before sacrifice.

RESULTS

Canonical Wnt signalling is physiologically active in proliferative compartment of colonic crypts

Previous studies have shown by experimental manipulation of the Wnt signalling cascade that canonical Wnt signalling regulates intestinal epithelial proliferation (Korinek et al., 1998; Pinto et al., 2003; Kuhnert et al., 2004; Sansom et al., 2004; Andreu et al., 2005; Fevr et al., 2007). However, whether canonical Wnt signalling is active in the proliferative compartment of normal colonic crypts remains unclear. To address this question, we separated actively proliferating progenitor cells (transit-amplifying cells) from non-proliferating cells in the colon by using transgenic mice that express a histone H2B-GFP fusion protein under the control of a tetracycline-responsive regulatory element (TRE) (Tumbar et al., 2004). H2B-GFP becomes incorporated or diluted in a cell cycle-dependent manner and thus facilitates the separation of frequently dividing cells from infrequently dividing cells in any given tissue,

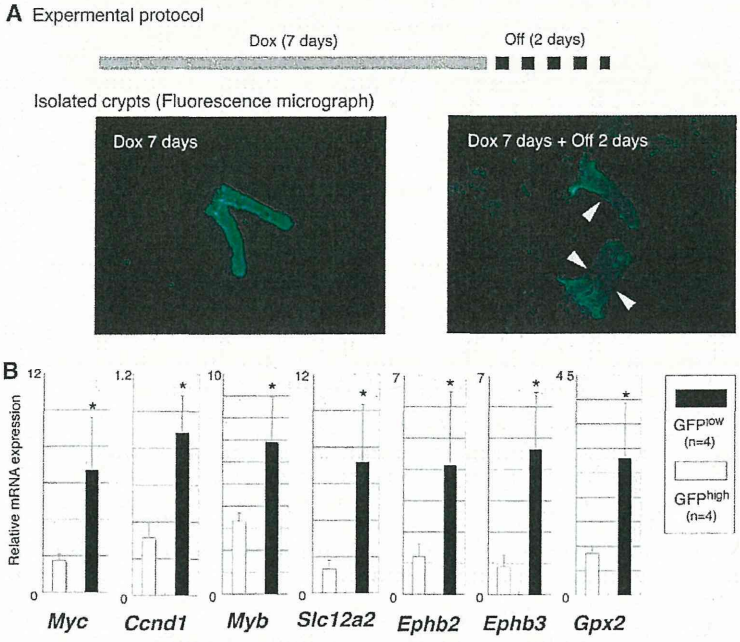

Fig. 1. Upregulation of canonical Wnt target genes in the proliferative compartments of colonic crypts. (**A**) Separation of proliferating cells from non-proliferative cells in the colon of histone H2B-GFP inducible mice. All crypt cells were labelled with nuclear GFP after Histone-GFP induction for 7 days, whereas the subsequent withdrawal of the induction resulted in dilution of the nuclear GFP signals in proliferating progenitor cells according to the cell divisions. Arrowheads indicate the decreased signal of the nuclear GFP at the proliferating compartments. (**B**) qRT-PCR for canonical Wnt target genes in GFP^{low} and GFP^{high} cells. After FACS sorting, the expression of canonical Wnt target genes was analysed by qRT-PCR. Expressions of *Myc*, *Ccnd1*, *Myb*, *Slc12a2*, *Ephb2*, *Ephb3* and *Gpx2* are significantly higher in GFP^{low} cells than in GFP^{high} cells. Data are mean ± s.d.; $^*P<0.05$, by Mann–Whitney *U*-test.

as has been successfully shown for the skin and haematopoietic system (Tumbar et al., 2004; Foudi et al., 2009). Specifically, H2B-GFP mice were crossed with mice harbouring a *Rosa26* promoter-driven M2 reverse tetracycline transactivator (M2rtTA) allele (Beard et al., 2006) to enable H2B expression in essentially all tissues. In the absence of doxycycline treatment, colonic epithelial cells exhibited no detectable GFP signals, thus excluding leaky expression of the transgene. By contrast, 7 days after doxycycline administration, all crypt cells exhibited a strong nuclear GFP signal (Fig. 1A). When doxycycline was withdrawn for 2 days after the initial labelling period, nuclear GFP signal was diluted in proliferating cells, consistent with rapid cell divisions of progenitor cells, whereas non-proliferating cells retained GFP (Fig. 1A). GFP^{high} non-proliferating and GFP^{low} proliferating epithelial cells were then sorted from the isolated crypts by FACS for subsequent molecular analyses (supplementary material Fig. S1A). To validate our approach to separate proliferating cells from non-proliferating cells using H2B-GFP dilution, we examined the expression levels of cell proliferation-related genes by microarray analysis. As expected, the expression of cyclins and Cdks, including *Ccna2*, *Ccnb1*, *Ccnd1*, *Ccnd2*, *Cdk2*, *Cdk4* and *Cdk6*, was higher in GFP^{low} cells than in GFP^{high} cells, whereas Cdk inhibitors, such as *Cdkn1a* and *Cdkn2b*, were found to be downregulated in GFP^{low} cells compared with GFP^{high} cells. Gene expression of candidates was validated by quantitative RT-PCR (supplementary material Fig. S1B). We also confirmed that GFP^{low} cells contained a higher number of Ki-67 (Mki67 – Mouse Genome Informatics)-positive cells than GFP^{high} cells by immunostaining colon sections of H2B-GFP mouse (supplementary material Fig. S1C). Importantly, we found that a number of canonical Wnt signalling target genes were upregulated in GFP^{low} proliferating cells compared with GFP^{high} non-proliferating cells using microarray analysis. qRT-PCR confirmed a significant upregulation of Wnt target genes (van de Wetering et al., 2002) (Fig. 1B), implying that canonical Wnt signalling is associated with active proliferation of progenitor cells in normal colonic crypts.

Forced induction of β-catenin leads to rapid *de novo* crypt formation in the colon

To investigate the effects of acute Wnt activation on adult intestinal homeostasis, we generated doxycycline-inducible β-catenin mice. This was achieved by targeting a constitutive active version of β-catenin (S33 mutation) under the control of a tetOP minimal promoter into the *Col1a1* locus in ES cells, which were subsequently injected into blastocysts to produce transgenic mice. Unless noted, homozygous transgenic mice were used in the experiment. When we fed adult mice doxycycline in the drinking water (2.0 mg/ml), β-catenin-induced animals became morbid after only 6-8 days. In the colon, 5 days of doxycycline treatment led to nuclear accumulation of β-catenin in the epithelium (Fig. 2A) and strong upregulation of canonical Wnt target genes such as *Myc* and *Ccnd1* (Fig. 2B). Notably, we frequently observed crypt fission and/or branching in β-catenin-induced colon sections, suggesting that the *de novo* crypt formation was induced by β-catenin induction (Fig. 2A). Immunohistological analyses of colon sections from doxycycline-induced chimeric mice demonstrated that the crypt fission/branching phenotype was only seen in β-catenin-induced crypts but not in host embryo-derived crypts, documenting a cell-autonomous effect of β-catenin induction (supplementary material Fig. S2A). We also observed an increase in crypt fission/branching in the crypts of the small intestine (supplementary material Fig. S2B). Analysis of isolated crypts confirmed that the fission and budding of crypts occurred at a significantly higher rate in β-catenin-induced colon than in non-induced colon (Fig. 2C,D). In addition, staining of sections for mucin with Alcian Blue-periodic acid-Schiff (AB-PAS) demonstrated a significant suppression of cellular differentiation towards goblet cells following β-catenin activation (supplementary material Fig. S3A). By contrast, chromogranin A-positive cells were found in both β-catenin-induced and non-induced crypts, showing a lesser effect on the enteroendocrine cell differentiation (supplementary material Fig. S3B). The numbers of chromogranin A-positive cells per crypt were 1.36±1.00 and 1.12±1.10 in β-catenin-induced and non-induced

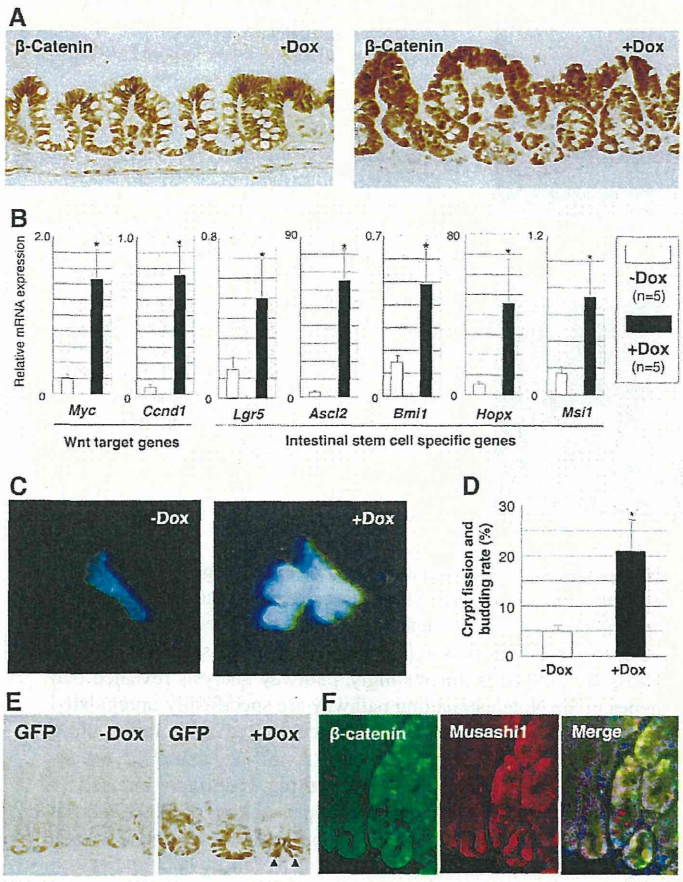

Fig. 2. β-Catenin induction leads to *de novo* crypt formation with increased expression of ISC markers in the colon. (**A**) β-Catenin immunostaining on colonic section of β-catenin-induced mice. Doxycycline treatment results in nuclear accumulation of β-catenin and frequent fission/budding of colonic crypts. (**B**) qRT-PCR for Wnt target genes and ISC-specific genes. The expression of Wnt target genes and ISC-specific genes are significantly upregulated by β-catenin induction. Data are mean ± s.d.; *P<0.05, by Mann–Whitney U-test. (**C**) Isolated colonic crypts from a doxycycline-treated mouse. A drastic crypt budding is observed in the crypt with β-catenin induction. (**D**) Fission/budding rate in isolated crypts from doxycycline-treated mice. Crypt fission/budding occurs at a significantly higher rate in doxycycline-treated mice than in non-treated mice. Data are mean ± s.d.; *P<0.05, by Mann–Whitney U-test. (**E**) Immunostaining for GFP on colonic sections of β-catenin-induced mice with *Lgr5-GFP* knock-in allele. GFP expression reveals an increased number of *Lgr5*-expressing cells at the lower part of colonic crypts in doxycycline-treated mice. Note that GFP-expressing cells are observed at the bottom of a bifurcating crypt (arrowheads). (**F**) Double immunostaining for Musashi1 (red) and β-catenin (green) on a colonic section of a doxycycline-treated chimeric mouse. Musashi1 expression is coincident with increased β-catenin expression.

colonic crypts, respectively, and no statistical significance was found between groups.

Barker et al. demonstrated that in the mouse gastrointestinal tract Lgr5 specifically labels active ISCs, which are located at the crypt base, cycle frequently and replenish the entire epithelium within a week (Barker et al., 2007). Consistent with the fact that *Lgr5* is a target of β-catenin/Tcf transcription (Barker et al., 2007), qRT-PCR demonstrated that β-catenin activation caused a significant increase in *Lgr5* expression (Fig. 2B). To determine whether the number of *Lgr5*-expressing cells has also increased in these mice, we crossed β-catenin-inducible mice with *Lgr5-GFP* knock-in mice, in which the *GFP* gene is regulated by the endogenous *Lgr5* promoter (Barker et al., 2007). Immunohistochemistry for GFP revealed that the number of *Lgr5*-expressing cells had indeed increased by 4.2-fold following β-catenin induction (Fig. 2E; supplementary material Fig. S4). Of note, although nuclear accumulation of β-catenin was observed throughout the crypt epithelium, expanded *Lgr5*-expressing cells were only observed at the lower part of the crypts (Fig. 2E; supplementary material Fig. S4A). This finding suggests that only existing ISCs, and possibly progenitor cells, respond to Wnt activation by producing more *Lgr5*-expressing cells whereas differentiated cells, located at the upper part of the crypts, are unresponsive to forced β-catenin expression. In addition to an increase in *Lgr5* expression, we also observed a strong upregulation of *Ascl2* (Fig. 2B), another active ISC-specific gene (van der Flier et al., 2009). As transgenic expression of *Ascl2* has been recently shown to induce ectopic crypt formation in the intestine (van der Flier et al., 2009), the increased levels of *Ascl2* might explain the observed crypt fission/budding phenotype in β-catenin-induced crypts. In addition to active ISCs, recent reports have indicated that quiescent ISCs are located at position 4 of the small intestine (Li and Clevers, 2010). Interestingly, β-catenin induction increased the expression of markers for the quiescent ISCs as well, including *Bmi1* and *Hopx* (Fig. 2B) (Sangiorgi and Capecchi, 2008; Takeda et al., 2011). Lastly, we examined the expression of Musashi1, a marker for putative stem and early progenitor cells (Potten et al., 2003), and found that β-catenin induction resulted in an upregulation of Musashi1 (Fig. 2B,F) in a cell-autonomous manner (Fig. 2F). Taken together, these data demonstrate that acute activation of β-catenin results in *de novo* crypt formation within a few days in a cell-autonomous fashion, accompanied by the amplification of ISC-like cells.

Colon cells with highest nuclear β-catenin do not actively divide

Previous studies have suggested that the canonical Wnt signalling plays a role in active cell proliferation of the intestine (Sansom et al., 2004; Andreu et al., 2005). In agreement, using the histone H2B-GFP mouse model, we show here that Wnt signalling is active in the proliferating progenitor compartment of normal colonic crypts under physiological conditions (Fig. 1B). To assess directly the effect of Wnt activation on the cell proliferation, we performed double-immunostaining with β-catenin and the proliferation marker Ki-67 on β-catenin-induced colonic sections. Unexpectedly, we found that the majority of cells with nuclear β-catenin failed to stain positively for Ki-67 (Fig. 3A). Instead, Ki-67 staining was

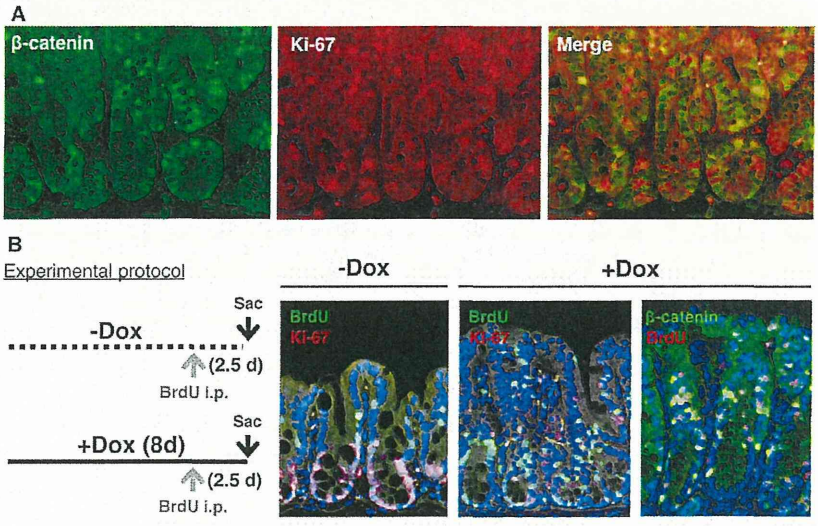

Fig. 3. Slow cycling properties of β-catenin-induced colonic cells. (**A**) Double immunostaining for β-catenin (green) and Ki-67 (red) on a β-catenin-induced colonic section. Majority of colonic cells with strong nuclear β-catenin expression are not coincident with Ki-67. (**B**) A scheme of the BrdU pulse-chase experiment and double immunostaining for Ki-67/BrdU and β-catenin/BrdU. In normal crypts, most proliferating progenitor cells have lost the BrdU retention according to the active cell divisions, and only a small number of cells retain BrdU. By contrast, β-catenin induction leads to an increased number of BrdU-retaining cells. Immunostaining for β-catenin (green) and BrdU (red) shows that BrdU-retaining cells frequently express nuclear β-catenin, indicating that colonic cells with strong nuclear β-catenin divide slowly. Sac, sacrifice.

predominantly observed in cells adjacent to cells with strong nuclear β-catenin signal (Fig. 3A). The majority of Ki-67-positive cells showed cytoplasmic and moderate β-catenin expression (76.7%) on the section, but some Ki-67-positive cells revealed nuclear and strong expression (23.3%). These observations were confirmed by a BrdU incorporation assay. When mice were injected with BrdU (100 mg/kg i.p.) 2 hours before sacrifice, the colonic cells with strong nuclear β-catenin showed less frequent BrdU incorporation (supplementary material Fig. S5A). We infer from this finding that intestinal cells with strong nuclear β-catenin expression did not actively divide. To investigate further the proliferation history of cells after β-catenin induction, we performed a pulse-chase experiment using BrdU (Fig. 3B). Mice were given a single BrdU injection (100 mg/kg i.p.) during the doxycycline treatment and were sacrificed 2 days later (Fig. 3B). β-Catenin induction caused an increased number of BrdU-retaining, i.e. non-dividing, cells near the crypt bottom, whereas non-induced crypts contained a small number of BrdU-retaining cells above the proliferative compartment (Fig. 3B). Furthermore, double-immunostaining for BrdU and β-catenin revealed that BrdU-retaining cells frequently expressed nuclear β-catenin (Fig. 3B). These results imply that, although forced β-catenin activation results in a net increase of cell proliferation in the colon, cells with strong nuclear β-catenin signal divide relatively slowly as measured by Ki-67 proliferation and BrdU label-retention assays. To support these findings, qRT-PCR revealed that the expression of the Cdk inhibitors *Cdkn1a*, *Cdkn1b* and *Cdkn1c* were significantly upregulated in β-catenin-induced colonic crypts (supplementary material Fig. S5B).

β-Catenin overexpression induces activation of Notch

In order to dissect further the molecular mechanisms underlying *de novo* crypt formation upon β-catenin induction, we compared the gene expression profiles of β-catenin-induced and non-induced colon crypts. Briefly, colonic crypts isolated from β-catenin-inducible control mice and from mice fed doxycycline for 5 days were subjected to microarray analysis. Consistent with our finding that β-catenin induction results in *de novo* crypt formation, microarray data confirmed the upregulation of ISC-specific genes, such as *Lgr5*, *Ascl2* and *Hopx*, as well as Wnt target genes in β-catenin-induced colon crypts (supplementary material Table S1).

Next, we wished to elucidate the apparent discrepancy between β-catenin-induced *de novo* crypt formation and the observed slow cycling properties of β-catenin-high cells. To this end, we compared gene expression profiles of β-catenin-induced cells and fast-cycling H2B-GFP low cells. Interestingly, pathway analysis revealed that genes in the Notch signalling pathway are specifically upregulated in β-catenin-induced colonic cells compared with fast-cycling normal crypt cells (Fig. 4A). qRT-PCR confirmed that *Hes1*, a well-established target gene of Notch signalling, is strongly induced by β-catenin activation with significant upregulation of Notch ligands (*Jag1* and *Jag2*) and Notch receptors (*Notch1* and *Notch2*) (Fig. 4B). Furthermore, we found that Notch ligands and Notch receptors were significantly upregulated as early as 12 hours after doxycycline treatment (Fig. 5B; see more details below). Consistent with this observation, immunohistochemical analysis revealed the strong nuclear expression of Hes1 on colonic sections of β-catenin-induced mice. (supplementary material Fig. S6). Our results suggest that β-catenin expression might activate Notch signalling through upregulation of its ligands and receptors.

Notch inhibition induces active cell proliferation in slow-cycling cells and blocks crypt fission and budding by β-catenin induction

In order to determine the relative contribution of activated Notch signalling to *de novo* crypt formation and the slow-cycling properties of colonic cells following β-catenin activation, we treated β-catenin-induced mice with a Notch/γ-secretase inhibitor (Fig. 4C). Surprisingly, treatment with a Notch inhibitor induced active proliferation of β-catenin-expressing, slow-cycling cells. Inhibitor-treated crypts were elongated with increased numbers of Ki-67 positive cells (Fig. 4D,E; supplementary material Fig. S7). Importantly, the simple withdrawal of doxycycline treatment (protocol G4) or the administration of Notch inhibitor alone (protocol G5) did not cause abnormal cell proliferation (Fig. 4E), indicating that constitutive Wnt activation is essential for active cell proliferation. To quantify the effect of Notch inhibition on cell proliferation in the presence of β-catenin activation, we performed a pulse-chase experiment with BrdU. Mice were given a single dose of BrdU (100 mg/kg i.p.) during the doxycycline treatment in the presence or absence of Notch inhibitor, and animals were sacrificed 2 days later. Immunohistochemical analysis showed that, in contrast

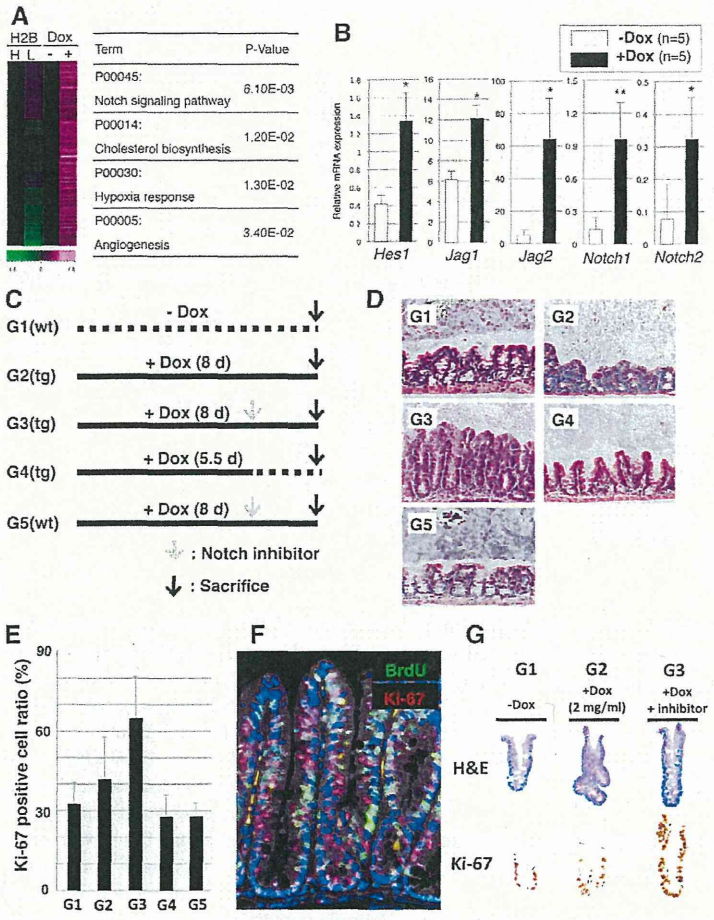

Fig. 4. Notch activation contributes to the maintenance of a slow-cycling state in β-catenin-induced colon. (**A**) Activation of Notch signalling pathway in β-catenin-induced slow-cycling colonic epithelium. Genes specifically upregulated in β-catenin-induced cells, but not in fast-cycling cells (GFP-Low cells in the H2B-GFP experiment) were selected. The heat map shows log2-fold changes in gene expression between β-catenin-induced and non-induced colon (right two columns in the left panel) and between histone-GFP-low and high cells (left two columns). The values for β-catenin non-induced colon and histone-GFP-high cells were used as normalisation for comparison, respectively. Subsequently, gene enrichment analysis were performed using DAVID on the selected genes and revealed that genes in a Notch signalling pathway are significantly concentrated in β-catenin-induced cells. All of the significantly enriched pathways in β-catenin-induced cells are listed in the table. H2B, histone H2B-GFP mouse; H, GFP^{high} cells; L, GFP^{low} cells; Dox, doxycycline treatment for β-catenin induction. (**B**) qRT-PCR analyses of Notch signalling related genes in β-catenin-induce colonic crypts. The Notch target *Hes1*, the Notch ligands *Jag1* and *Jag2*, and the Notch receptors *Notch1* and *Notch2* are strongly upregulated in β-catenin-activated crypts. Data are means ± s.d.; $*P<0.05$, $**P<0.01$, by Mann–Whitney *U*-test. (**C**,**D**) Experimental protocols for treatment with the Notch inhibitor (C) and the representative histology in each group (D). A Notch inhibitor was administrated orally at 2 days prior to sacrifice. (**E**) The Notch inhibitor induces active proliferation in β-catenin-induced colon. Ki-67-positive cell ratio (percentage of Ki-67-positive cells) is significantly higher in G3 than in other groups ($P<0.00001$ for G1, G4 and G5, and $P<0.0005$ for G2, by one-way ANOVA and Turkey's post hoc test, respectively). (**F**) BrdU pulse-chase experiment in mice treated with doxycycline and Notch inhibitor (protocol G3). Double immunostaining for BrdU (green) and Ki-67 (red) on a colon section. The Notch inhibitor reduces BrdU-retention in colonic crypts, whereas it increases Ki-67-positive cells throughout the crypt. (**G**) H&E staining and Ki-67 immunostaining of isolated crypts. The Notch inhibitor induces active cell proliferation and suppressed the *de novo* crypt formation in β-catenin induced crypts.

to the increased number of BrdU-retaining cells following β-catenin induction alone (Fig. 3B), combined treatment with doxycycline and the Notch inhibitor reduced the number of BrdU-retaining nuclei, whereas it increased the number of Ki-67-positive cells (Fig. 4F). These findings suggest that treatment with the Notch inhibitor induces proliferation of slow-cycling cells that have accumulated as a consequence of β-catenin expression. Importantly, treatment of β-catenin-induced mice with the Notch inhibitor also normalised crypt fission and budding rates (Fig. 4G; supplementary material Fig. S8A), which was accompanied by decreased nuclear β-catenin expression without a change in gene expression at the mRNA level (supplementary material Fig. S8B,C). These results indicate that Notch activation contributes to the maintenance of a slow-cycling state and to *de novo* crypt formation in β-catenin-induced colon, and, hence, Notch inhibition turns slow-cycling cells into fast-cycling cells in the context of transgenic β-catenin expression. However, in spite of the clear morphological changes, we could not detect a change in gene expression of the Notch target